PNAS
www.pnas.org

Supplementary Information for

Identification of SLAC1 anion channel residues required for CO_2/bicarbonate sensing and regulation of stomatal movements

Jingbo Zhang[1], Nuo Wang[2], Yinglong Miao[2,4*], Felix Hauser[1], J. Andrew McCammon[2], Wouter-Jan Rappel[3], Julian I. Schroeder[1*]

Julian I. Schroeder
Email: jischroeder@ucsd.edu

Yinglong Miao
Email: miao@ku.edu

This PDF file includes:

Supplementary text
Figs. S1 to S6
References for SI reference citations

www.pnas.org/cgi/doi/10.1073/pnas.1807624115

Supplementary Information Text

Supplemental Methods:

Electrophysiological Analyses

Two-electrode voltage-clamp in *Xenopus* oocytes

Oocytes were isolated by Collagenase D (30 mg/ml) (Roche Diagnostics, catalog No. 11088882001) digestion from the surgically extracted ovaries of *Xenopus laevis* frogs supplied by Ecocyte Bioscience (Austin, Texas) (catalog number: 0-100-2) and Nasco (Fort Atkinson, Wisconsin) (product number LM00935). Prior to cRNA injection, isolated oocytes were incubated in ND96 buffer (1 mM $CaCl_2$, 1 mM $MgCl_2$, 96 mM NaCl, 10 mM MES/Tris, pH=7.5. Osmolarity was adjusted to 220 mM by D-sorbitol) overnight for recovery. cRNA of OST1, SLAC1 and its derivatives were generated from linearized plasmids by using the mMESSAGE mMACHINE® T7 Kit (Thermo Fisher Scientific) as previously described (1). SLAC1yc and OST1yn represent C-terminal fusions to YFP halves, which enables SLAC1 activation (2). 11.5 ng cRNA of each protein were co-injected into oocytes and incubated in ND96 buffer at 16 °C for 2 days prior to two-electrode voltage clamp recordings. Oocyte voltage clamp recordings were applied in a buffer (1 mM $CaCl_2$, 2 mM KCl, 24 mM NaCl, 70 mM Na-gluconate, 10mM MES/Tris, pH=7.4. Osmolarity was adjusted to 220 mM by D-sorbitol) with a Cornerstone (Dagan) TEV-200 amplifier and a Digidata 1440A low-noise data acquisition system using pClamp software (Molecular Devices). For analyses of HCO_3^- regulation of SLAC1 currents, $NaHCO_3$ was injected into oocytes to achieve a bicarbonate concentration of 11.5 mM (3, 4) and we waited for 20 min prior to recording as described elsewhere (5). Steady state currents were recorded with 3-s voltage pulses ranging from +40 mV to -160 mV in -20 mV decrements with a holding potential at 0 mV.

As shown previously, the time-dependent kinetics at hyperpolarized voltages of S-type currents in guard cells and SLAC1-mediated currents in oocytes vary showing either time-dependent relaxation or more instantaneous currents (1, 5, 6). Therefore, H_2O-injected control oocyte recordings were

interspersed during all oocyte batches and consistently showed only very small background currents. The magnitude of ionic currents varies from one oocyte batch to another due to protein expression level variation among batches of oocytes (5). To avoid time-of-measurement and inter-batch dependence in the data, we included the indicated controls in each batch of oocytes and control oocytes were recorded intermittently with the investigated conditions. Moreover, experiments were repeated in at least three independent batches of oocytes showing consistent conclusions. Data from one representative oocyte batch are shown with controls from the same batch in each figure panel as described previously (5).

Patch clamp of guard cell protoplasts

Guard cell protoplasts from WT (Col-0) and *slac1-1* transformed lines expressing SLAC1-WT and SLAC1-R256A were isolated by enzymatic digestion as described elsewhere (7, 8). 3 to 4 detached leaves were blended twice with deionized water at room temperature for approximately 30 seconds and epidermal tissue were collected using a 100 µm nylon mesh. By using 10 mL enzyme solution containing 1% (wt/vol) Cellulase R-10 (Yakult, Japan), 0.5% (wt/vol) Macerozyme R-10 (Yakult, Japan), 0.1 mM KCl, 0.1 mM $CaCl_2$, 485 mM D-mannitol, 0.5% (wt/vol) BSA, 0.1% (wt/vol) kanamycin sulfate and 10 mM ascorbic acid, pH adjusted to 5.6 with Tris, protoplasts were released after 16 h digestion at 25 °C on a shaker with 40 rpm speed. After filtration through a 10 µm nylon mesh, guard cell protoplasts were collected by centrifugation at 200×g for 10 minutes. The protoplasts were washed twice with a wash solution containing 0.1 mM KCl, 0.1 mM $CaCl_2$ and 500 mM D-sorbitol, pH = 5.6 adjusted with KOH. Guard cell protoplasts were re-suspended in the washing solution on ice prior to patch clamping.

S-type anion channel currents were recorded with an Axon 200B amplifier (Axon instruments), a Digidata 1440A low-noise data acquisition system and Clampex 10.2 software. Recordings were conducted 3 to 5 min after the whole cell configuration was achieved. During recordings, the membrane voltage was pulsed from +35 mV to -145 mV for 3 seconds with -30 mV decrements with a

holding of +30 mV. The pipette solution contained: 150 mM CsCl, 5.86 mM $CaCl_2$, 6.7 mM EGTA, 2 mM $MgCl_2$, 5 mM Mg-ATP, 10 mM HEPES. pH 7.1 adjusted with Tris. The osmolarity was adjusted to 500 mOsm with D-sorbitol. The bath solution contained: 30 mM CsCl, 2 mM $MgCl_2$, 1 mM $CaCl_2$, 10 mM MES. pH 5.6 adjusted with Tris. The osmolarity was adjusted to 485 mOsm with D-sorbitol. 13.5 mM $CsHCO_3$ was freshly added into the pipette solution and the pH verified at 7.1 for HCO_3^- activated S-type anion channel current recordings. Guard cell protoplasts were pre-incubated for 20 min with 50 μM ABA in the bath solution prior to recording for ABA-activated S-type anion channel current recordings. Liquid junction potentials were measured and corrected when larger than ± 2 mV.

SLAC1 model system

A model of the SLAC1 channel structure was generated using the crystal structure of the *H. influenzae* TehA homolog (9) as template and applying three separate modeling algorithms: ModBase, iTasser and RaptorX (10-12). By using the MatchMaker function provided in Chimera, the quality of the SLAC1 structure modeling was determined as following:

ModBase SLAC1 - TehA RMSD between 288 pruned atom pairs is 0.452 angstroms; (across all 310 pairs: 1.327)

iTasser: SLAC1 - TehA RMSD between 14 pruned atom pairs is 1.245 angstroms; (across all 299 pairs: 20.600)

Raptor: SLAC1 - TehA RMSD between 244 pruned atom pairs is 0.273 angstroms; (across all 311 pairs: 3.103)

The homology model of the transmembrane region of the SLAC1 structure (residues E179 – F504) generated by ModBase was used in the present study and coordinates for this model are available at (https://modbase.compbio.ucsf.edu/modbase-cgi/model_details.cgi?searchmode=default&displaymode=moddetail&seq_id=&model_id=04b1be492cab72cdb6b456ce3c84685a&queryfile=1524763690_9474).

The SLAC1 structure was then submitted to the online CHARMM-GUI Membrane Builder (http://www.charmm-gui.org/) for addition of the Palmitoyl-oleoyl

phosphatidylcholine (POPC) lipids and a 0.15M KCl solution (34 K^+ ions and 42 Cl^- ions were added to neutralize the system, resulting in a final ionic strength of 0.15 M). About 10 mM bicarbonate (3) (i.e., 3 bicarbonate molecules) were added to the system afterwards by replacing water molecules. The final simulation system of SLAC1 measured HCO_3^- interaction probability with SLAC1 over a volume of 83 × 83 × 105 $Å^3$ with a total of ~65,000 atoms. Periodic boundary conditions were applied to the system (13).

Gaussian Accelerated Molecular Dynamics

Gaussian accelerated molecular dynamics (GaMD) enhances the conformational sampling of large biomolecules by adding a harmonic boost potential to reduce energy barriers during conformation changes of proteins (14). Details of the method have been described in previous studies (15, 16) and a brief summary is provided here. When the system potential $V(\vec{r})$ is lower than a reference energy *E*:

$$V^*\left(\vec{r}\right) = V\left(\vec{r}\right) + \Delta V\left(\vec{r}\right)$$

$$\Delta V\left(\vec{r}\right) = \begin{cases} \frac{1}{2}k\left(E - V\left(\vec{r}\right)\right)^2, & V\left(\vec{r}\right) < E \\ 0, & V\left(\vec{r}\right) \geq E, \end{cases} \quad (1)$$

where *k* is the harmonic force constant and $V(\vec{r})$ is a function of the atomic coordinates. The two adjustable parameters *E* and *k* are automatically determined based on three enhanced sampling principles (15). The reference energy needs to be set in the following range:

$$V_{\max} \leq E \leq V_{\min} + \frac{1}{k}, \quad (2)$$

where $V_{\min}$ and $V_{\max}$ are the system minimum and maximum potential energies. To ensure that Eqn. (2) is valid, k has to satisfy: $k \leq \frac{1}{V_{\max} - V_{\min}}$. We defined for $k \equiv k_0 \bullet \frac{1}{V_{\max} - V_{\min}}$, then $0 < k_0 \leq 1$. The standard deviation of ΔV needs to be

small enough (i.e., narrow distribution) to ensure accurate energetic reweighting (17): $\sigma_{\Delta V} = k\left(E - V_{avg}\right)\sigma_V \le \sigma_0$, where V_{avg} and σ_V are the average and standard deviation of the system potential energies, $\sigma_{\Delta V}$ is the standard deviation of ΔV with σ_0 as a user-specified upper limit (e.g., 10k_BT) for accurate reweighting. When *E* is set to the lower bound $E = V_{\max}$ according to Eqn. (2), k_0 can be calculated as:

$$k_0 = \min\left(1.0, k_0'\right) = \min\left(1.0, \frac{\sigma_0}{\sigma_V} \bullet \frac{V_{\max} - V_{\min}}{V_{\max} - V_{avg}}\right). \tag{3}$$

Alternatively, when the threshold energy *E* is set to its upper bound $E = V_{\min} + \frac{1}{k}$, k_0 is set to:

$$k_0 = k_0'' \equiv \left(1 - \frac{\sigma_0}{\sigma_V}\right) \bullet \frac{V_{\max} - V_{\min}}{V_{avg} - V_{\min}}, \tag{4}$$

if k_0'' is found to lie between *0* and *1*. Otherwise, k_0 is calculated using Eqn. (3).

For energetic reweighting of GaMD simulations, the probability distribution along a selected reaction coordinate $A(\boldsymbol{r})$ is written as $p^*(A)$, where $\boldsymbol{r}$ denotes the atomic positions $\{\boldsymbol{r}_1, \cdots, \boldsymbol{r}_N\}$. Given the boost potential $\Delta V(\boldsymbol{r})$ of each frame, $p^*(A)$ can be reweighted to recover the canonical ensemble distribution, $p(A)$, as:

$$p(A_j) = p^*(A_j) \frac{\left\langle e^{\beta \Delta V(\boldsymbol{r})} \right\rangle_j}{\sum_{i=1}^{M} \left\langle p^*(A_i) e^{\beta \Delta V(\boldsymbol{r})} \right\rangle_i}, \; j = 1, \cdots, M, \tag{5}$$

where *M* is the number of bins, $\beta = k_B T$ and $\left\langle e^{\beta \Delta V(\boldsymbol{r})} \right\rangle_j$ is the ensemble-averaged Boltzmann factor of $\Delta V(\boldsymbol{r})$ for simulation frames found in the jth bin. As shown

earlier (17), when the boost potential follows a near-Gaussian distribution, cumulant expansion to the second order provides a more accurate reweighting than the exponential average and Maclaurin series expansion methods (17). The ensemble-averaged reweighting factor is approximated using cumulant expansion (18, 19):

$$\left\langle e^{\beta\Delta V}\right\rangle = \exp\left\{\sum_{k=1}^{\infty}\frac{\beta^k}{k!}C_k\right\}, \tag{6}$$

where the first two cumulants are given by:

$$\begin{aligned} C_1 &= \left\langle \Delta V\right\rangle, \\ C_2 &= \left\langle \Delta V^2\right\rangle - \left\langle \Delta V\right\rangle^2 = \sigma_{\Delta V}^2 \end{aligned} \tag{7}$$

The reweighted free energy $F\left(A\right) = -k_B T \ln p\left(A\right)$ is calculated as:

$$F\left(A\right) = F^*\left(A\right) - \frac{1}{\beta}\sum_{k=1}^{2}\frac{\beta^k}{k!}C_k + F_c, \tag{8}$$

where $F^*\left(A\right) = -k_B T \ln p^*\left(A\right)$ is the modified free energy obtained from GaMD simulation and F_c is a constant.

Simulation Protocol

The GaMD implemented in NAMD 2.11 (16) was applied to simulate bicarbonate interactions with the SLAC1 anion channel. Standard CHARMM36 force field parameters were used for the protein and POPC lipids (20), the CHARMM36 General Force Field was used for bicarbonate (21), and the TIP3P model for the water molecules (22). For the bicarbonate, force field, parameters were retrieved from the CHARMM General Force Field (CGenFF) databases. A cutoff distance of 12 Å was used for van der Waals and short-range electrostatic interactions and long-range electrostatic interactions were computed with the particle-mesh Ewald summation method (23) using a grid point density of 1/Å. A 2 femtosecond integration time-step was used for all molecular dynamics simulations and a multiple-time-stepping algorithm (24) was employed with bonded and short-range nonbonded interactions computed every time-step and long-range electrostatic

interactions were computed every two time-steps. The SHAKE (25) algorithm was applied to all hydrogen-containing bonds.

Simulations of SLAC1 started with equilibration of the lipid tails (13). With all other atoms fixed, the lipid tails were energy minimized for 1000 steps using the conjugate gradient algorithm and melted with an NVT run for 0.5 *ns* at 300 K. The systems were further equilibrated using an NPT run at 1 atm and 300 K for 10 *ns* with 5 kcal/(mol·Å^2) harmonic position restraints applied to the crystallographically-identified atoms in the protein and ligand. The system volume was found to decrease with a flexible unit cell applied and level off during the second half of the 10 *ns* NPT run, suggesting that that water molecules, ions and lipids were well equilibrated surrounding the channel protein. Final equilibration of the two systems was performed using an NPT run at 1 atm and 300 K for 0.5 *ns* with all atoms unrestrained. After these minimization and equilibration procedures, conventional MD simulations were performed on the systems for 100 *ns* at 1 atm pressure and 300 K with a constant ratio constraint applied on the lipid bilayer in the X-Y plane (13). GaMD simulation was then performed using the dual-boost scheme with the threshold energy E set to V_{max}. The GaMD simulations included 2 ns cMD, 30 ns equilibration after adding the boost potential and then three independent 100 ns production runs with randomized atomic velocities.

Stomatal density and index analyses

The fifth mature leaves of 4 to 6 week-old plants that were at the same stage as those that were used for gas exchange analyses, were detached and incubated overnight or longer in buffer containing 7:1 ethanol : acetic acid. These cleared leaves were softened for 30 min in 1M potassium hydroxide and rinsed twice with water. Leaves were mounted on slides with 15% glycerol and images of abaxial epidermal surfaces were taken using DIC (differential interference contrast) microscopy (Leica DM5000B) at ×40 magnification and guard cell and pavement cell numbers were counted using Image J software as previously described (26).

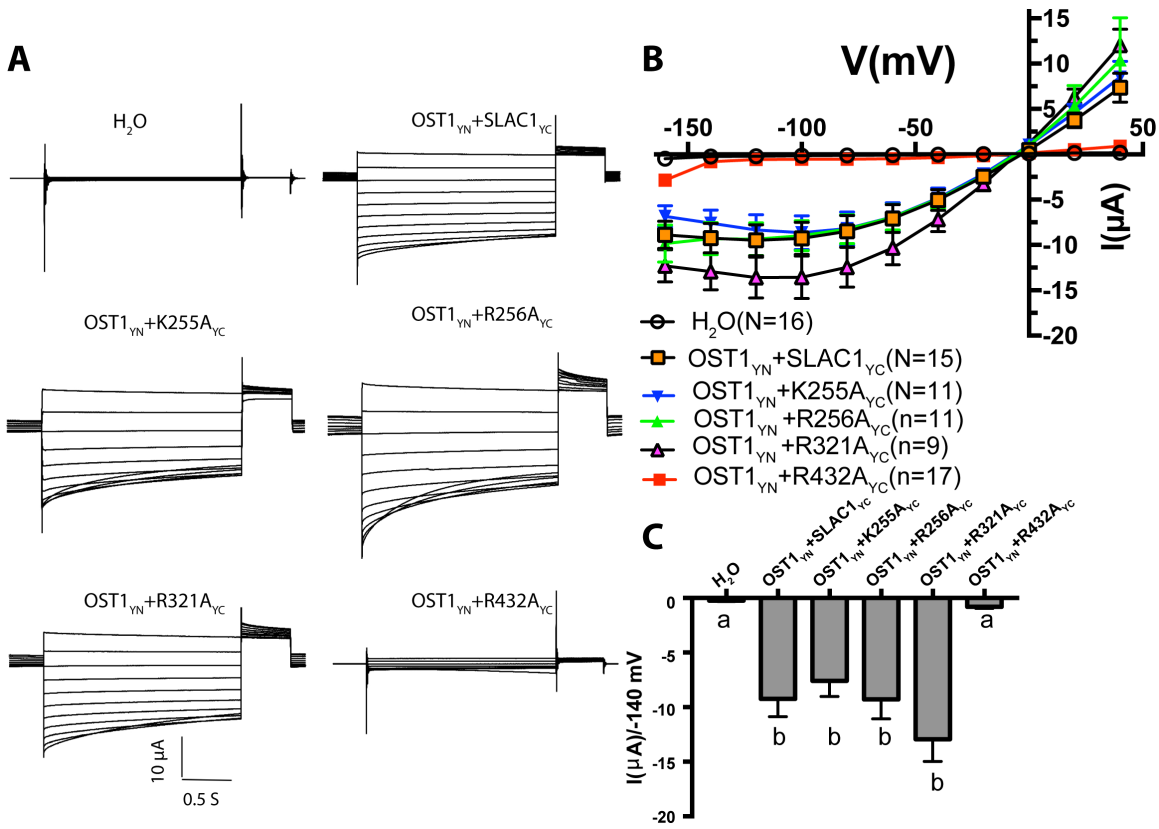

Fig. S1 Impact of mutations on channel activity of SLAC1 in *Xenopus* oocytes

(A) Representative whole cell Cl^- current recordings in oocytes co-expressing SLAC1yc isoforms with the OST1yn protein kinase. Currents were recorded in response to 3s voltage pulses ranging from +40 mV to -160 mV in -20 mV steps with a holding potential at 0 mV and return to +40 mV after pulses. The bath solution contained: 10 mM Mes/Tris (pH=7.4), 1 mM $MgCl_2$, 1 mM $CaCl_2$, 2mM HCl, 24 mM NaCl and 70 mM Na-gluconate. (B) Mean current-voltage curves of oocytes co-expressing the indicated proteins. (C) Average currents of the indicated SLAC1 isoforms at -140 mV. All oocytes were recorded from the same batch. Four batches of oocytes showed similar results (n= 9 to 17 oocytes from each oocyte batch per condition). Error bars denote mean ± s.e.m. Means with different letters are grouped based on one-way ANOVA and Tukey's test, $P < 0.05$.

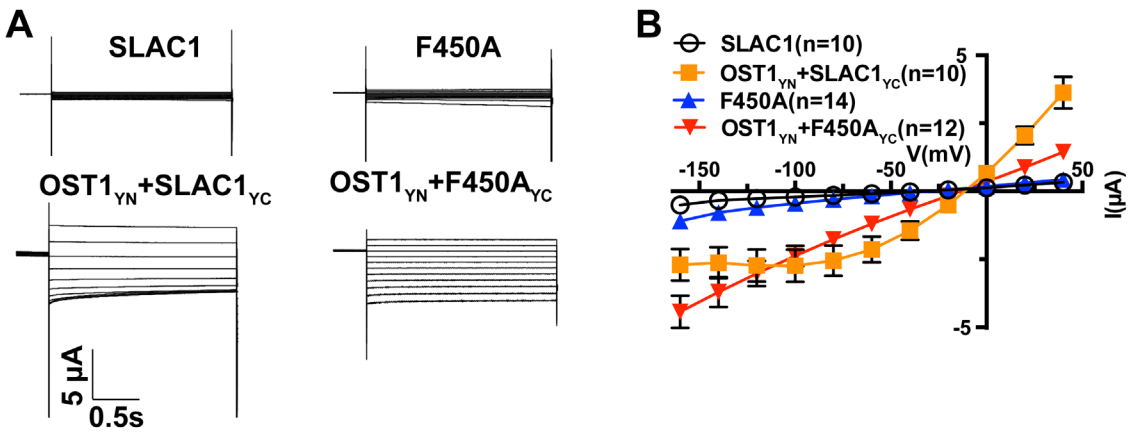

Fig. S2 Impact of F450 mutation on SLAC1 channel activity (A) Representative whole cell current recordings in oocytes co-expressing SLAC1yc or SLAC1yc-F450A with OST1yn protein kinase. Currents were recorded in response to 3s voltage pulses ranging from +40 mV to -160 mV in -20 mV steps with a holding potential at 0 mV. (B) Mean current-voltage curves of oocytes co-expressing the indicated proteins. Error bars denote mean ± s.e.m. Three independent batches of oocytes showed similar results (n=10 to 14 oocytes from each oocyte batch per condition).

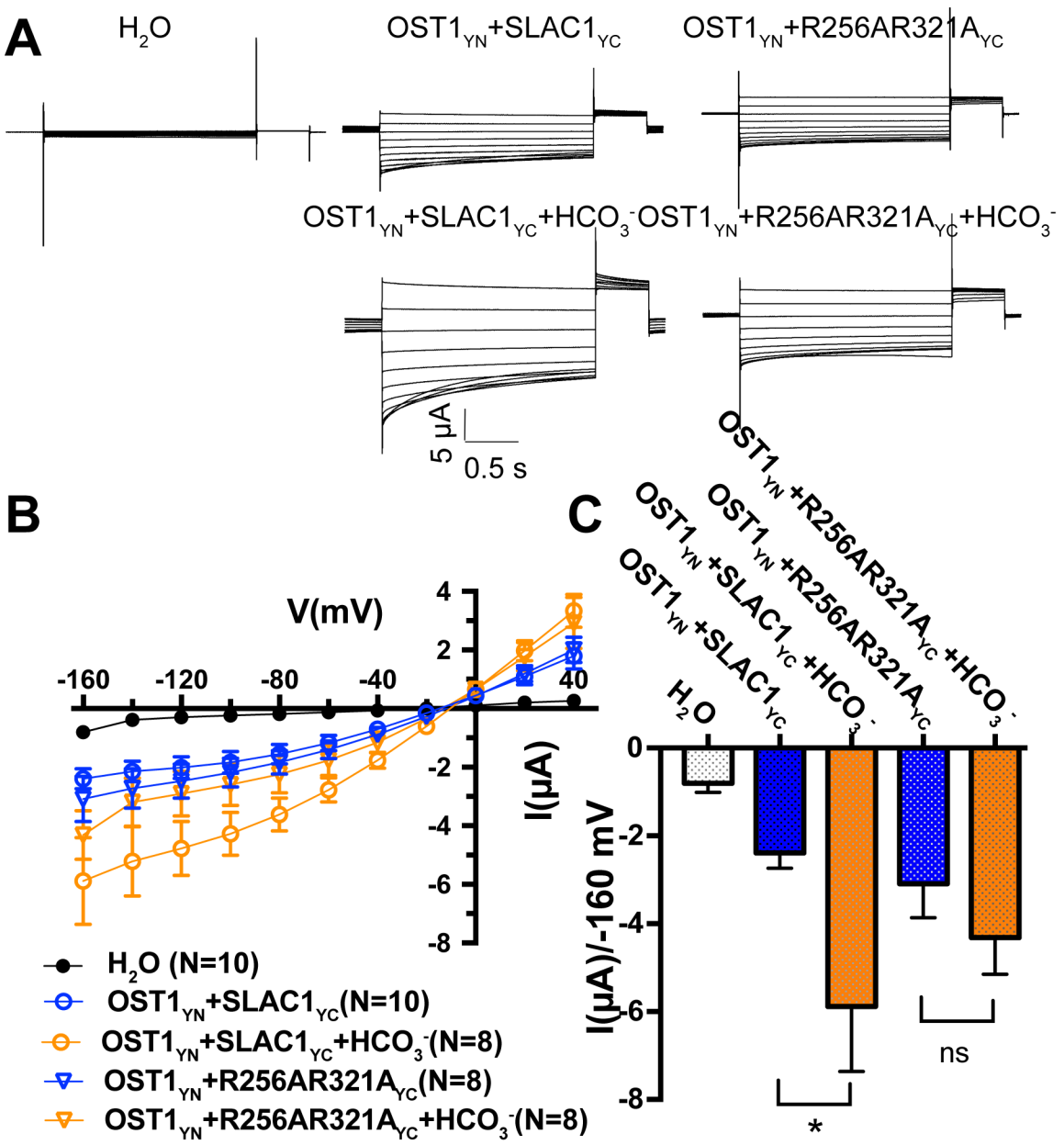

Fig. S3 Impact of R256A-R321A double mutation on bicarbonate enhancement of SLAC1-mediated currents

(A) Representative whole cell Cl^- current recordings in oocytes co-expressing SLAC1yc or SLAC1-R256A-R321Ayc with OST1yn. Currents were recorded in response to 3s voltage pulses ranging from +40 mV to -160 mV in -20 mV steps with a holding potential at 0 mV followed by 40 mV after voltage pulses. (B) Mean current-voltage curves of oocytes co-expressing the indicated proteins with or without $NaHCO_3$ injection. (C) Average currents of the indicated SLAC1 isoforms

with and without injection of 11.5 mM bicarbonate at -160 mV. Three independent batches of oocytes showed similar results (n= 8 to 10 oocytes from each oocyte batch per condition). Error bars denote mean ± s.e.m. ($P<0.05$, OST1yn+SLAC1yc vs OST1yn+SLAC1yc+HCO_3^-; $P=0.29$, OST1yn+R256A-R321Ayc vs OST1yn+R256A-R321Ayc +HCO_3^-, student's t-test)

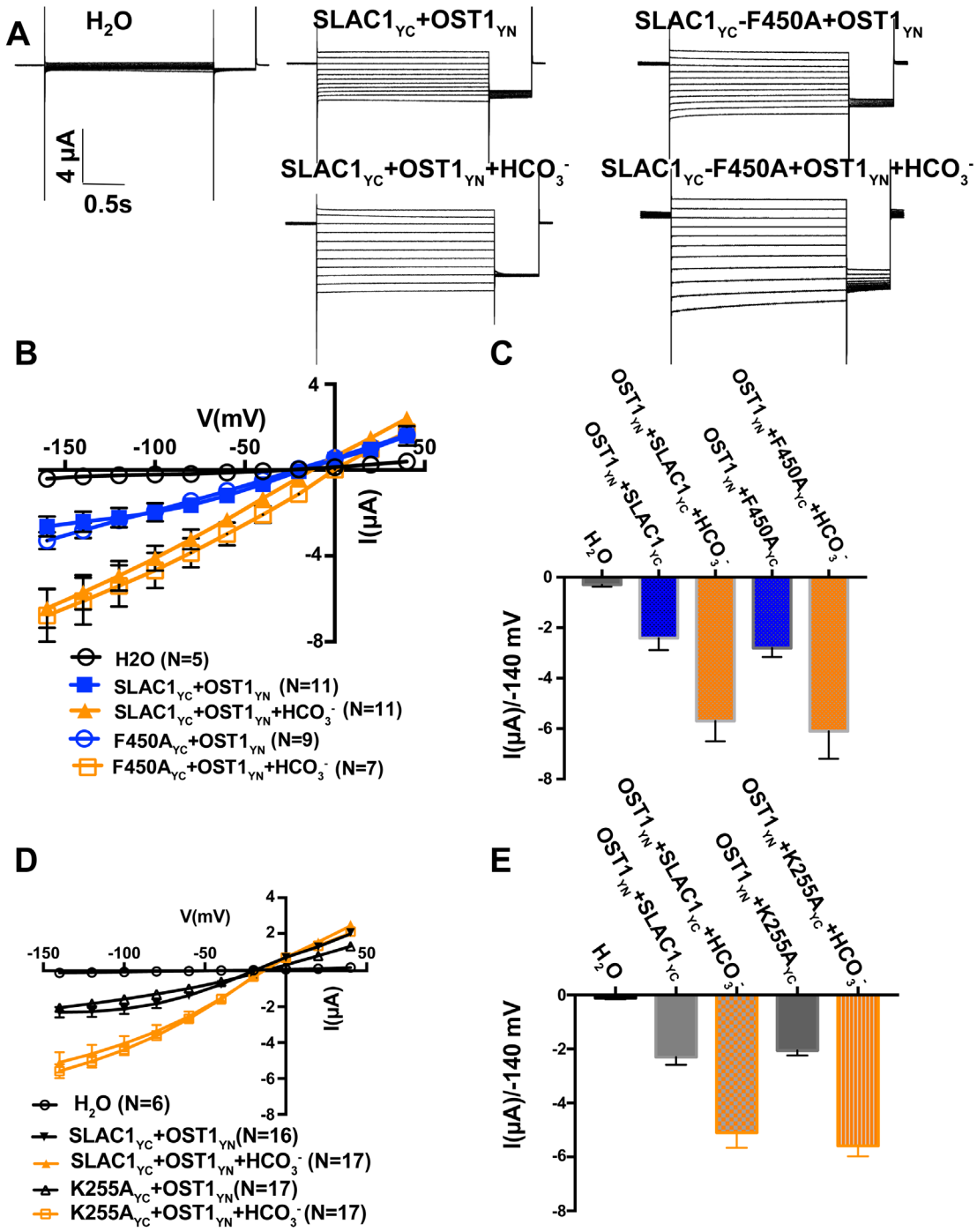

Fig. S4 Mutations of SLAC1 residue F450 and K255 have no impact on bicarbonate enhancement of anion currents (A) Representative whole cell ion current recordings in oocytes co-expressing SLAC1yc or SLAC1-F450Ayc with OST1yn. Currents were recorded in response to 3s voltage pulses ranging from +40 mV to -160 mV in -20 mV steps with a holding potential of 0 mV and return to -120 mV after voltage pulses. (B) and (C) Mean current-voltage curves and average currents at -140 mV of oocytes co-expressing the indicated proteins with and without injection of 11.5 mM bicarbonate. (D) and (E) Mean current-voltage

curves and average currents at -140 mV of oocytes co-expressing OST1yn with SLAC1yc or SLAC1-K255Ayc with and without injection of 11.5 mM bicarbonate. Error bars denote mean ± s.e.m. Three independent batches of oocytes showed similar results (n=5 to 17 oocytes for each oocyte batch per condition).

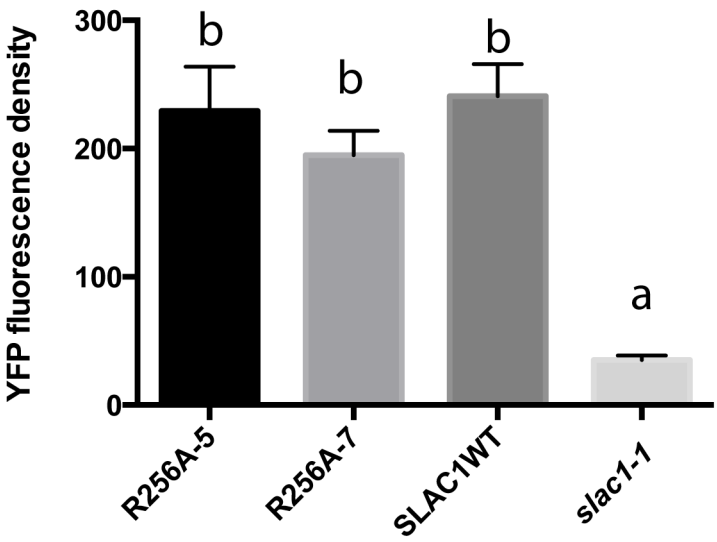

Fig. S5 mVENUS fluorescence intensity in guard cells of SLAC1 transformed plants and *slac1-1*

Average mVENUS fluorescence intensities were determined by using ImageJ software. 20-30 stomata were analyzed in each line. One-way Anova and Tukey's multiple comparisons showed that: SLAC1pro::SLAC1-R256A-5 vs SLAC1pro::SLAC1-R256A-7, P=0.8; SLAC1pro::SLAC1-R256A-5 vs SLAC1pro::SLAC1-WT, P=0.9; SLAC1pro::SLAC1-R256A-7 vs SLAC1pro::SLAC1-WT, P= 0.5; *slac1-1* vs SLAC1pro::SLAC1-WT, P<0.001; *slac1-1* vs SLAC1pro::SLAC1-R256A-5, P<0.01; *slac1-1* vs SLAC1pro::SLAC1-R256A-5, P<0.05. Error bars denote mean ± s.e.m. (3 to 4 leaves per condition)

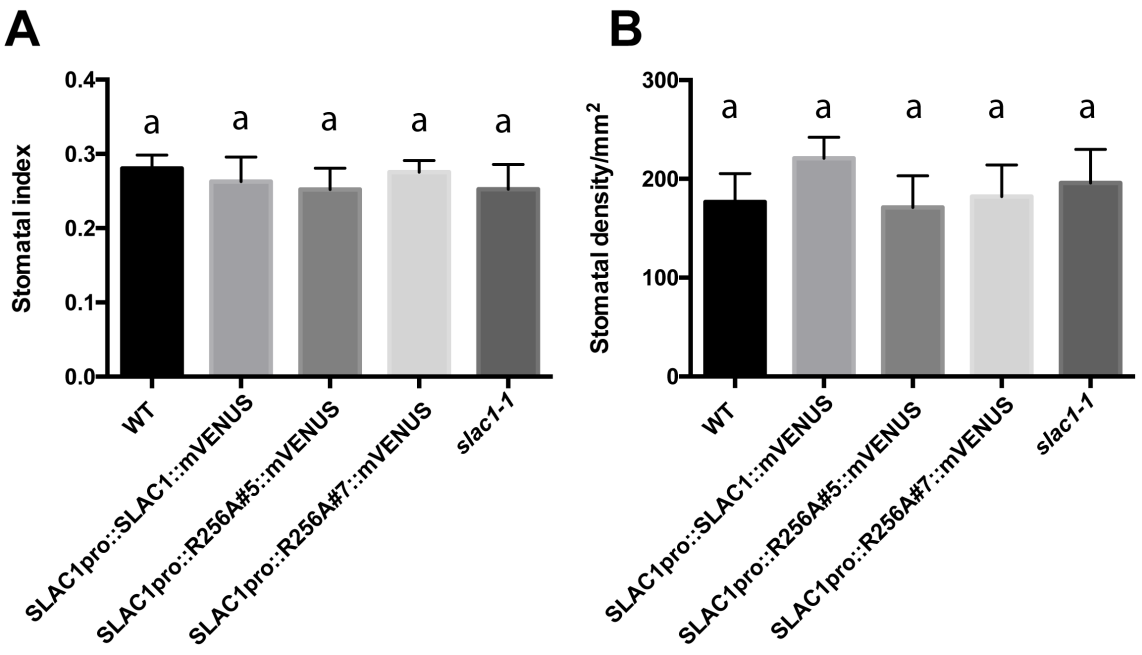

Fig. S6 Stomatal density analyses of *slac1* transformed lines
Average stomatal index (A) and stomatal density (B) of the abaxial side of the fifth true leaves of 4 to 6 week-old plants. Plants were of the same age as used for stomatal conductance response analyses (WT, n=7; SLAC1pro::SLAC1::mVENUS, n=9; SLAC1pro::R256A#5::mVENUS, n=9; SLAC1pro::R256A#7::mVENUS, n=8; *slac1-1*, n=6 leaves each from separate plants). One-way ANOVA and Tukey's multiple comparisons test show that no significant differences were observed in both stomatal index and stomatal density in these lines. Data are mean ± SEM.

References

1. Wang C, Zhang J, & Schroeder JI (2017) Two-electrode Voltage-clamp Recordings in Xenopus laevis Oocytes: Reconstitution of Abscisic Acid Activation of SLAC1 Anion Channel via PYL9 ABA Receptor. *Bio-protocol* 7(2).
2. Geiger D*, et al.* (2009) Activity of guard cell anion channel SLAC1 is controlled by drought-stress signaling kinase-phosphatase pair. *Proceedings of the National Academy of Sciences of the United States of America* 106(50):21425-21430.
3. Xue S*, et al.* (2011) Central functions of bicarbonate in S-type anion channel activation and OST1 protein kinase in CO2 signal transduction in guard cell. *The EMBO journal* 30(8):1645-1658.
4. Tian W*, et al.* (2015) A molecular pathway for CO2 response in Arabidopsis guard cells. *Nat Commun* 6.
5. Wang C*, et al.* (2016) Reconstitution of CO2 Regulation of SLAC1 Anion Channel and Function of CO2-Permeable PIP2;1 Aquaporin as CARBONIC ANHYDRASE4 Interactor. *Plant Cell* 28(2):568-582.
6. Horak H*, et al.* (2016) A Dominant Mutation in the HT1 Kinase Uncovers Roles of MAP Kinases and GHR1 in CO2-Induced Stomatal Closure. *Plant Cell* 28(10):2493-2509.
7. Brandt B*, et al.* (2015) Calcium specificity signaling mechanisms in abscisic acid signal transduction in Arabidopsis guard cells. *eLife* 4.
8. Yamamoto Y*, et al.* (2016) The Transmembrane Region of Guard Cell SLAC1 Channels Perceives CO2 Signals via an ABA-Independent Pathway in Arabidopsis. *Plant Cell* 28(2):557-567.
9. Chen YH*, et al.* (2010) Homologue structure of the SLAC1 anion channel for closing stomata in leaves. *Nature* 467(7319):1074-U1157.
10. Pieper U*, et al.* (2014) ModBase, a database of annotated comparative protein structure models and associated resources. *Nucleic Acids Res* 42(D1):D336-D346.
11. Yang JY*, et al.* (2015) The I-TASSER Suite: protein structure and function prediction. *Nat Methods* 12(1):7-8.
12. Kallberg M*, et al.* (2012) Template-based protein structure modeling using the RaptorX web server. *Nat Protoc* 7(8):1511-1522.
13. Miao YL*, et al.* (2016) Accelerated structure-based design of chemically diverse allosteric modulators of a muscarinic G protein-coupled receptor. *Proceedings of the National Academy of Sciences of the United States of America* 113(38):E5675-E5684.
14. Miao YL, Feher VA, & McCammon JA (2015) Gaussian Accelerated Molecular Dynamics: Unconstrained Enhanced Sampling and Free Energy Calculation. *J Chem Theory Comput* 11(8):3584-3595.
15. Miao Y, Feher VA, & McCammon JA (2015) Gaussian Accelerated Molecular Dynamics: Unconstrained Enhanced Sampling and Free Energy Calculation. *J. Chem. Theory Comput.* 11(8):3584-3595.

16. Pang YT, Miao Y, Wang Y, & McCammon JA (2017) Gaussian Accelerated Molecular Dynamics in NAMD. *J. Chem. Theory Comput.* 13(1):9-19.
17. Miao Y, Sinko W, Pierce L, Bucher D, & McCammon JA (2014) Improved reweighting of accelerated molecular dynamics simulations for free energy calculation. *J. Chem. Theory Comput.* 10(7):2677–2689.
18. Hummer G (2001) Fast-growth thermodynamic integration: Error and efficiency analysis. *J. Chem. Phys.* 114(17):7330-7337.
19. Eastwood MP, Hardin C, Luthey-Schulten Z, & Wolynes PG (2002) Statistical mechanical refinement of protein structure prediction schemes: Cumulant expansion approach. *J. Chem. Phys.* 117(9):4602-4615.
20. Klauda JB*, et al.* (2010) Update of the CHARMM All-Atom Additive Force Field for Lipids: Validation on Six Lipid Types. *The Journal of Physical Chemistry B* 114(23):7830-7843.
21. Vanommeslaeghe K*, et al.* (2010) CHARMM general force field: A force field for drug-like molecules compatible with the CHARMM all-atom additive biological force fields. *J Comput Chem* 31(4):671-690.
22. Jorgensen WL, Chandrasekhar J, Madura JD, Impey RW, & Klein ML (1983) Comparison of Simple Potential Functions for Simulating Liquid Water. *J. Chem. Phys.* 79(2):926-935.
23. Essmann U*, et al.* (1995) A Smooth Particle Mesh Ewald Method. *J. Chem. Phys.* 103(19):8577-8593.
24. Phillips JC*, et al.* (2005) Scalable molecular dynamics with NAMD. *Journal of Computational Chemistry* (26):1781-1802.
25. Ryckaert J-P, Ciccotti G, & Berendsen HJC (1977) Numerical integration of the cartesian equations of motion of a system with constraints: molecular dynamics of n-alkanes. *J. Comput. Phys.* 23(3):327-341.
26. Engineer CB*, et al.* (2014) Carbonic anhydrases, EPF2 and a novel protease mediate CO2 control of stomatal development. *Nature* 513(7517):246-250.